Physics Letters B 811 (2020) 135984

Contents lists available at ScienceDirect

Physics Letters B

www.elsevier.com/locate/physletb

Measurements of the induced polarization in the quasi-elastic $A(e, e'\vec{p})$ process in non-coplanar kinematics

A1 Collaboration

S.J. Paul [a,*,1], T. Kolar [b], T. Brecelj [b], P. Achenbach [c], H. Arenhövel [c], A. Ashkenazi [a], J. Beričič [b], R. Böhm [c], D. Bosnar [d], E. Cline [e], E.O. Cohen [a], L. Debenjak [b], M.O. Distler [c], A. Esser [c], I. Friščić [d,2], R. Gilman [e], C. Giusti [f], M. Heilig [g], M. Hoek [c], D. Izraeli [a], S. Kegel [c], P. Klag [c], Y. Kohl [c], I. Korover [h,a], J. Lichtenstadt [a], I. Mardor [a,i], H. Merkel [c], D.G. Middleton [c], M. Mihovilovič [k,b,c], J. Müller [c], U. Müller [c], M. Olivenboim [a], E. Piasetzky [a], J. Pochodzalla [c], G. Ron [j], B.S. Schlimme [c], M. Schoth [c], F. Schulz [c], C. Sfienti [c], S. Širca [k,b], R. Spreckels [c], S. Štajner [b], S. Strauch [l], M. Thiel [c], A. Tyukin [c], A. Weber [c], I. Yaron [a]

[a] School of Physics and Astronomy, Tel Aviv University, Tel Aviv 69978, Israel
[b] Jožef Stefan Institute, 1000 Ljubljana, Slovenia
[c] Institut für Kernphysik, Johannes Gutenberg-Universität, 55099 Mainz, Germany
[d] Department of Physics, University of Zagreb, HR-10002 Zagreb, Croatia
[e] Rutgers, The State University of New Jersey, Piscataway, NJ 08855, USA
[f] Dipartimento di Fisica, Università degli Studi di Pavia and INFN, Sezione di Pavia, via A. Bassi 6, I-27100 Pavia, Italy
[g] Universität Konstanz, Fachbereich Physik, Universitätsstraße 10, 78464 Konstanz, Germany
[h] Department of Physics, NRCN, P.O. Box 9001, Beer-Sheva 84190, Israel
[i] Soreq NRC, Yavne 81800, Israel
[j] Racah Institute of Physics, Hebrew University of Jerusalem, Jerusalem 91904, Israel
[k] Faculty of Mathematics and Physics, University of Ljubljana, 1000 Ljubljana, Slovenia
[l] University of South Carolina, Columbia, SC 29208, USA

ARTICLE INFO

Article history:
Received 11 August 2020
Received in revised form 24 November 2020
Accepted 24 November 2020
Available online 30 November 2020
Editor: D.F. Geesaman

ABSTRACT

We report measurements of the induced polarization $\vec{P}$ of protons knocked out from ^{2}H and ^{12}C via the $A(e, e'\vec{p})$ reaction. We have studied the dependence of $\vec{P}$ on two kinematic variables: the missing momentum $p_{\rm miss}$ and the "off-coplanarity" angle ϕ_{pq} between the scattering and reaction planes. For the full 360° range in ϕ_{pq}, both the normal (P_y) and, for the first time, the transverse (P_x) components of the induced polarization were measured with respect to the coordinate system associated with the scattering plane. P_x vanishes in coplanar kinematics, however in non-coplanar kinematics, it is on the same scale as P_y.

We find that the dependence on ϕ_{pq} is sine-like for P_x and cosine-like for P_y. For carbon, the magnitude of the induced polarization is especially large when protons are knocked out from the $p_{3/2}$ shell at very small $p_{\rm miss}$. For the deuteron, the induced polarization is near zero at small $|p_{\rm miss}|$, and its magnitude increases with $|p_{\rm miss}|$. For both nuclei such behavior is reproduced qualitatively by theoretical results, driven largely by the spin-orbit part of the final-state interactions. However, for both nuclei, sizeable discrepancies exist between experiment and theory.

1. Introduction

Within the shell model a spin-orbit term is required in the mean-field potential of atomic nuclei in order to explain the energy splitting of the single-particle levels for reproducing the magic numbers [1–3]. The spin-orbit interaction also plays an im-

* Corresponding author.
E-mail address: paulsebouh@mail.tau.ac.il (S.J. Paul).
[1] Present address: UC-Riverside, Riverside, CA 92521, USA.
[2] Present address: MIT-LNS, Cambridge, MA 02139, USA.

https://doi.org/10.1016/j.physletb.2020.135984

portant role in optical potentials which describe scattering processes. These have a strong influence in the final-state interactions (FSI) affecting quasi-free $A(e,e'\vec{p})$ scattering [4–8], as well as various other types of scattering processes [9–12].

In elastic ep scattering, within the one-photon-exchange approximation, the induced polarization of the proton vanishes. Consequently, it is the FSI which in the $A(e,e'\vec{p})$ reaction gives rise to a non-vanishing induced polarization of the knocked-out proton. In view of the fact that it is largely insensitive to details of the nucleon electromagnetic form factors, the induced polarization serves as an effective probe of FSI effects in quasi-elastic $A(e,e'\vec{p})$. Here we present measurements of the induced polarization of quasi-elastic protons from ^{2}H and ^{12}C over a wide range in the missing momentum, $p_{\rm miss}$.

Previous measurements of the normal component, P_y, of the induced polarization have been performed at MIT-Bates on ^{2}H [13] at low $p_{\rm miss}$ and ^{12}C with large $p_{\rm miss}$ in coplanar kinematics [14]. Measurements of P_y were also performed on ^{4}He at Jefferson Lab (JLab) [15,16] over a wide $p_{\rm miss}$ range.

In Ref. [14], it was found that the induced polarizations of protons knocked out from the s shell of ^{12}C show a different behavior from those knocked out of the p shell. This difference was attributed to the spin-orbit ($L\cdot S$) interaction. The measured values of P_y for ^{2}H at low $p_{\rm miss}$ in [13] were much smaller than those measured for other nuclei in [14–16]. All measurements prior to those reported here were restricted to almost-coplanar geometry.

The induced polarization measurements presented here were performed at the Mainz Microtron (MAMI), during four run periods from 2012-2017. Our measurements for both nuclei cover a large range in $p_{\rm miss}$, and the full 360° range in the off-coplanarity angle, ϕ_{pq} (See Fig. 1). Calculations predict a dependence of the induced polarization on ϕ_{pq} largely due to the $L\cdot S$ interaction which hitherto has remained unexplored. Our ^{2}H data greatly extend the range in $p_{\rm miss}$ compared to the previous measurements in [13], while our ^{12}C data significantly improve the statistical precision and the range in ϕ_{pq} compared to the existing data [14]. Furthermore, we measure not only the normal component, P_y, but also, for the first time, the transverse component, P_x, which vanishes in coplanar kinematics ($\phi_{pq}=0°$ or 180°). The *transferred* polarizations measured in our experiments were reported in [17–19] for ^{2}H and [20–22] for ^{12}C.

Section 2 describes the experimental setup, the measured reaction, and the kinematic settings. The data analysis and extraction of the induced polarization are described in Sec. 3. The details of theoretical calculations, to which we compare our data, are given in Sec. 4. We then present the data for both nuclei and their dependence on ϕ_{pq} and $p_{\rm miss}$ in Secs. 5 and 6, and conclude in Sec. 7.

2. Experimental setup and kinematics

The experiments were performed at MAMI using the A1 beamline and spectrometers [23]. For these measurements, a 600-690 MeV polarized continuous-wave electron beam was used. The beam current was ≈10 μA. Due to the frequent flipping of the beam helicity (about 1 Hz), the average beam polarization in our event sample is zero, as verified by internal checks on the data.

The targets used for the ^{2}H and ^{12}C measurements were a 50 mm long oblong cell filled with liquid deuterium [17–19] and a set of three 0.8 mm-thick graphite foils [20–22], respectively. We also performed calibration runs using a liquid hydrogen target.

Two high-resolution, small-solid-angle spectrometers with momentum acceptances of 20-25% were used to detect the scattered electrons and knocked-out protons in coincidence. Each of these spectrometers consists of an momentum-analyzing magnet system followed by a set of vertical drift chambers (VDCs) for tracking,

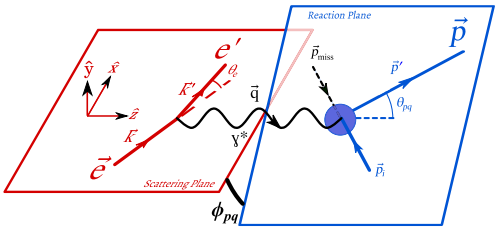

Fig. 1. Kinematics of the reaction with the definitions of the kinematic variables.

and a scintillator system for triggering and defining the time coincidence between the two spectrometers.

The proton spectrometer was equipped with a focal-plane polarimeter (FPP) with a 3-7 cm thick carbon analyzer and a set of horizontal drift chambers (HDCs) [23,24]. The spin-dependent scattering of the polarized proton by the carbon analyzer allows the determination of the proton polarization at the focal plane. The polarization at the interaction point is then determined by correcting for the spin precession in the spectrometer's magnetic field [24]. More details of the experiment can be found in [17–22].

The kinematics of the measured reactions are shown in Fig. 1. The electron's initial and final momenta are $\vec{k}$ and $\vec{k}'$ respectively, which define the scattering plane of the reaction. The reaction plane is defined by the momentum transfer $\vec{q}=\vec{k}-\vec{k}'$ and the recoiling proton's momentum $\vec{p}\,'$. We refer to the angle between the scattering plane and the reaction plane as the "off-coplanarity" angle of the reaction, denoted by ϕ_{pq}.

Following the convention of [15], we express the components of the induced polarization $\vec{P}$ in the scattering-plane coordinate system, such that $\hat{y}$ is normal to the scattering plane (along the direction of $\vec{k}\times\vec{k}'$), $\hat{z}$ is along the direction of the momentum transfer $\vec{q}$, and $\hat{x}=\hat{y}\times\hat{z}$, forming a right-handed coordinate system.

The missing momentum $\vec{p}_{\rm miss}\equiv\vec{q}-\vec{p}\,'$ is the recoil momentum of the residual nuclear system. Neglecting FSI, $-\vec{p}_{\rm miss}$ is equal to the initial momentum of the emitted proton, $\vec{p}_i$. We conventionally define positive and negative signs for $p_{\rm miss}$ by the sign of $\vec{p}_{\rm miss}\cdot\vec{q}$.

Our ^{2}H measurements were performed at six kinematic settings, labeled A through F, with varying ranges of $p_{\rm miss}$ and invariant four-momentum transfers $Q^2=-q^2$. Settings A and F were both centered at $p_{\rm miss}=0$, and have $Q^2=0.40$ (GeV/c)^2. Settings B and E covered large positive $p_{\rm miss}$, at $Q^2=0.40$ and 0.65 (GeV/c)^2, respectively. Settings C and D covered small and large negative $p_{\rm miss}$, respectively, and were both at $Q^2=0.18$ (GeV/c)^2. Details are given in Table 1.

Our ^{12}C measurements were taken at two kinematic settings. The first is the same Setting A of the deuteron measurements (centered near $p_{\rm miss}=0$, at $Q^2=0.40$ (GeV/c)^2). The second is Setting G, which covered a region of large negative $p_{\rm miss}$ at $Q^2=0.18$ (GeV/c)^2; this is similar to Setting D of the deuteron measurements, except with a different beam energy and the other kinematic variables modified accordingly.[3]

In each of the kinematic settings presented in this work, the spectrometers' reference trajectories form a parallel reaction ($\vec{p}\,'\parallel\vec{q}$). However, due to the spectrometer acceptance, our data sample included reactions with θ_{pq} (the angle between $\vec{p}$ and $\vec{q}$) up to ≈ 8°, with the full 360° range in the off-coplanarity angle ϕ_{pq}.

[3] In our earlier publications [20–22] on ^{12}C, this setting is referred to as Setting B. We refer to this setting as Setting G in this work in order to distinguish it from the Setting B of the deuteron measurements.

Table 1
The kinematic settings in the ^{2}H$(\vec{e}, e'\vec{p})$ and ^{12}C$(\vec{e}, e'\vec{p})$ measurements. The angles and momenta represent the central values for the two spectrometers: p_p and θ_p (p_e and θ_e) are the knocked out proton (scattered electron) momentum and scattering angles, respectively. The number of events passing the event selection cuts are also given.

		Kinematic setting						
		A	B	C	D	E	F	G
E_{beam}	[MeV]	600	600	630	630	690	690	600
Q^2	[(GeV/c)^2]	0.40	0.40	0.18	0.18	0.65	0.40	0.18
p_{miss}	[MeV/c]	−80 to 75	75 to 175	−80 to −15	−220 to −130	60 to 220	−70 to 70	−250 to −100
p_e	[MeV/c]	384	463	509	398	464	474	368
θ_e	[deg]	82.4	73.8	43.4	49.4	90.9	67.1	52.9
p_p	[MeV/c]	668	495	484	665	656	668	665
θ_p	[deg]	−34.7	−43.3	−53.3	−39.1	−33.6	−40.8	−37.8
Nucleus	shell	# of events passing cuts ($\times 10^3$)						
^{2}H		68	19	438	201	10	232	–
^{12}C	$s_{1/2}$	268	–	–	–	–	–	274
^{12}C	$p_{3/2}$	160	–	–	–	–	–	436

3. Data analysis

3.1. Event selection

Software cuts were applied to the data, in order to ensure good tracking, time coincidence, and event quality. These cuts applied here are identical to those of the earlier publications [17–22] on the transferred polarization, unless otherwise noted below. The full list of these cuts from the earlier analyzes, is listed in the supplementary material.

We applied additional tracking cuts to the proton's trajectory, requiring it to be within the part of the spectrometer where the precession of the proton's spin is well known and the false asymmetry could be determined using dedicated elastic ep measurements. In order to reduce false asymmetries, we also removed events where, if the proton had scattered in the azimuthally opposite direction in the carbon analyzer, it would either be outside of the geometric acceptance of the detector or hit a malfunctioning channel of the HDCs. Additionally, the polar angle Θ_{FPP} of the secondary scattering was required to be greater than 8° in order to avoid spin-independent Coulomb-scattering events, and less than 23° in order to improve the stability of the false-asymmetry determination (see note in supplementary material).

Following [17–19], we required the missing mass of the ^{2}H$(e, e'\vec{p})$ reaction to be consistent with the mass of a neutron. For the ^{12}C sample, we distinguish between protons knocked out from the s and p shells, following [20–22], by using cuts on the missing energy, E_{miss} in the reaction, defined as [25]:

$$E_{\text{miss}} \equiv \omega - T_p - T_{^{11}\text{B}}, \tag{1}$$

where $\omega = k^0 - k'^0$ is the energy transfer, T_p is the measured kinetic energy of the outgoing proton, and $T_{^{11}\text{B}}$ is the calculated kinetic energy of the recoiling residual system, assuming it is ^{11}B in the ground state. For the s-shell sample, we used the cut $30 < E_{\text{miss}} < 60$ MeV, while for the p-shell sample, we used $15 < E_{\text{miss}} < 25$ MeV [20–22].

The p-shell cut accepts events in which the residual $A-1$ system is left in one of several discrete states, including the ground-state of ^{11}B as well as a few excited states. The s-shell selection cut is much wider, comprising a broad range within the continuum of unbound residual $A-1$ states.

3.2. Polarization fitting

Before extracting the values of P_x and P_y for ^{2}H and ^{12}C, we first determined the false asymmetry using elastic ep events (for which the induced polarization is expected to be zero). This was accomplished by maximizing the log likelihood

$$\log \mathcal{L} = \sum_{\text{events}} \log \left[1 + \vec{A}^{\,\text{T}} \cdot \begin{pmatrix} -\sin\Phi_{\text{FPP}} \\ \cos\Phi_{\text{FPP}} \\ 0 \end{pmatrix} \right], \tag{2}$$

for the ep event sample, where Φ_{FPP} is the azimuthal angle of the secondary scattering and $\vec{A}$ is the false asymmetry in the focal plane coordinate system, parameterized as

$$\vec{A} = \begin{pmatrix} a_0^x + a_1^x \phi_{\text{vth}} \\ a_0^y + a_1^y \theta_{\text{vth}} \\ 0 \end{pmatrix}, \tag{3}$$

where θ_{vth} and ϕ_{vth} are the incident angles of the proton trajectory extrapolated from the VDCs to the HDCs. a_0^x, a_1^x, a_0^y, and a_1^y are the fitted coefficients. We then extracted the induced polarization for ^{2}H and ^{12}C by maximizing the log likelihood

$$\log \mathcal{L} = \sum_{\text{events}} \log \left[1 + (a\mathbf{S} \cdot \vec{P} + \vec{A})^{\text{T}} \cdot \begin{pmatrix} -\sin\Phi_{\text{FPP}} \\ \cos\Phi_{\text{FPP}} \\ 0 \end{pmatrix} \right], \tag{4}$$

where $\mathbf{S}$ is the calculated spin-transfer matrix for the proton trajectory of the event, and a is the analyzing power of the event (as determined by [26,27]). $\vec{P}$ is the induced polarization. We constrain P_z to be zero in order to improve the stability of our fit. This constraint has a negligible effect on the fitted P_x and P_y except in bins with very poor statistics.

The corrections for false asymmetry are larger for P_x than for P_y; the r.m.s. values of these corrections are ≈0.20 and ≈0.04 respectively. This is because $|A_y|$ is generally larger than $|A_x|$, and the off-diagonal terms of the spin-transfer matrix, S_{xy} and S_{yx}, dominate over the much smaller diagonal terms S_{xx} and S_{yy}. Details of the false-asymmetry determination, and the checks we used to validate its long-term stability, may be found in the supplementary material.

3.3. Systematic errors

The systematic errors in these measurements are due to a few sources, which are presented in Table 2. They are dominated by the uncertainty on the false asymmetry of the FPP. This is due to the limited statistics of the elastic ep sample used to determine this false asymmetry, and it contributes 0.012 to the systematic error on our corrected results for ^{2}H and ^{12}C.

The analyzing power of the carbon secondary scatterer is known to about 1% in this kinematic region [24,26,27]. It leads to a relative error of the same size on each component of $\vec{P}$. The uncertainty on the precession of the proton's spin introduces an additional 0.4% relative error. The systematic error due to the uncertainty of the alignment between the HDC and the VDC detector

Table 2
Sources of systematic errors on P_x and P_y. We distinguish between sources of systematic errors that do not scale with P_y (absolute errors), and those that do (relative errors). The total systematic errors are then $\Delta P_x = \sqrt{\Delta P^2_{x,\mathrm{abs}} + (\Delta P_{x,\mathrm{rel}} P_x)^2}$ and similarly for ΔP_y.

	$\Delta P_{x,\mathrm{abs}}$	$\Delta P_{y,\mathrm{abs}}$	$\Delta P_{xy,\mathrm{rel}}$
False asymmetry	0.010	0.012	–
Software cuts	0.005	0.006	–
Detector alignment	< 0.001	< 0.001	–
Kinematic setting	0.001	0.001	–
Precession	–	–	0.4%
Analyzing power	–	–	1.0%
Total	0.011	0.013	1.1%

systems was investigated to be less than 0.001, absolute, for both components. This was determined by repeating the analysis with each of the alignment parameters modified by plus or minus its uncertainty. In a similar manner, we estimate the uncertainty on both components due to the uncertainty on the kinematic settings (i.e. the beam energy and the two spectrometers' angles and momenta) to be about 0.001.

The software cuts, described in Sec. 3.1, introduce an additional absolute uncertainty of ≈0.006 to the overall systematic error. This was determined by performing slightly tighter cuts on each of the software cuts and then extracting the polarization as described above. The systematic uncertainty due to the cuts is then the quadrature sum of the deviations between the measured polarizations with each of the tightened cuts as compared to the standard set of cuts.

4. Calculations

For comparison, theoretical calculations of the induced polarization for ^{2}H and ^{12}C have been performed. For ^{2}H we have used a non relativistic calculation [28] including a realistic nucleon-nucleon (NN) potential, meson-exchange (MEC) and isobar (IC) currents, and relativistic contributions (RC) of leading order. For the bound and scattering states the realistic Argonne V_{18} potential [29] has been taken. As nucleon electromagnetic form factors we used the parameterizations from [30].

For ^{12}C, calculations were performed using a program [7] based on the relativistic distorted-wave approximation (RDWIA) where the FSI between the outgoing proton and the residual nucleus are described by a phenomenological relativistic optical potential. The original program [7] was modified [22] in order to account for non-coplanar kinematics, by including all relevant structure functions [6]. In the RDWIA calculations, only the one-body electromagnetic nuclear current is included. We chose the current operator corresponding to the cc2 definition [31], and we used the same parametrization of the nucleon form factors [30] as in the ^{2}H calculations. The relativistic proton bound-state wave functions were obtained from the NL-SH parametrization [32] and the scattering states from the so-called "democratic" parameterization of the optical potential [33]

We found that for both nuclei, the calculated induced polarization has very little sensitivity to the details of the nucleon form factors. A change of 10% to the form-factor ratio G_E/G_M in the calculations affects the induced polarization by less than 0.005.

In order to examine the influence of the $L \cdot S$ interaction on the induced polarization, we repeated these calculations while switching off this part of the potential. As we will show in Secs. 5 and 6, the $L \cdot S$ interaction is the dominant source of the induced polarization.

5. Dependence on off-coplanarity

In order to study the off-coplanarity behavior of the induced polarization, we performed fits of the polarization components P_x and P_y as functions of ϕ_{pq}. We present first the off-coplanarity behavior measured for ^{2}H and ^{12}C for each kinematic set over the entire measured p_{miss} range. The ϕ_{pq} dependence affects the integration in each p_{miss} bin as discussed below in Sec. 6.

The results for ^{2}H at the negative p_{miss} settings (C and D) are shown in Fig. 2. The statistical (systematic) uncertainties are shown as error bars (gray band). These are the only settings for which we observe a significant dependence of the induced polarization on ϕ_{pq}. In these settings, the P_x component has an oscillatory sine-like behavior, with an amplitude of about 0.1. The P_y component, on the other hand, shows no statistically significant dependence on ϕ_{pq} in any of the ^{2}H settings. For completeness, the results the other settings which cover the $p_{\mathrm{miss}} \approx 0$ and positive p_{miss} regions are shown in Fig. S2 of the supplementary material. For Settings B and E (positive p_{miss}) some ϕ_{pq} dependence cannot be excluded, however, the limited statistics do not allow us to draw a firm conclusion.

The data are compared to the calculations, which were performed using the kinematic parameters of a sample of the events in each bin (solid black curves). The calculations underestimate the amplitude of the ϕ_{pq} dependence of P_x for the two settings where this component is statistically significant. For P_y, the calculations, similar to the data, predict very little variation of with respect to ϕ_{pq}. The calculations were repeated with the $L \cdot S$ part of the potential switched off (green dashed curves), which causes the calculated polarization to nearly vanish, indicating that the induced polarization is due to the $L \cdot S$ part of the potential. We discuss the comparison between the data and calculations in further detail in Sec. 6, where both are compared as functions of p_{miss}.

The results for ^{12}C are shown in Fig. 3. The polarization components P_x (left-hand side) and P_y (right-hand side) were determined for each data set, both for s- (top panels) and p-shell protons (middle and bottom panels). The P_x components for both shells have an oscillatory sine-like dependence on ϕ_{pq}, similar to that of the deuteron (although with a larger amplitude). While the s-shell knockout data show no significant variation between the two kinematic settings, one notes for the p-shell knockout a sizable difference in the amplitudes, significantly larger in the low-p_{miss} region (Setting A).

The P_y component for the s-shell protons shows no strong dependence on ϕ_{pq} (similar to the ^{2}H data), with $P_y \approx -0.03$ over the entire p_{miss} region. On the other hand, one notes for p-shell protons quite a different behavior for P_y between the two settings, A and G. While at low p_{miss} (Setting A) P_y has a pronounced cosine-like ϕ_{pq} dependence with a sizable amplitude, it is fairly flat and small (≈ -0.05) in the higher $|p_{\mathrm{miss}}|$ region (Setting G).

The calculation of the induced polarization for ^{12}C was also performed using the kinematics and statistics of the data samples in each bin. For the P_x component, the theory predicts much smaller polarizations compared to the measured data with one exception. For s-shell knockout the calculations, like the data, display an almost identical behavior for both settings with a sine-like dependence. However, the predicted polarizations are much smaller with an opposite sign to the data. For p-shell knockout the situation is different. While the calculated P_x shows for Setting A at least a qualitative agreement although with a slightly smaller amplitude, the theory predicts an almost vanishing P_x for Setting G.

With respect to P_y, it is interesting to note that for p-shell knockout the calculation is in very good agreement with the data for both settings, predicting the same ϕ_{pq} dependence as well as

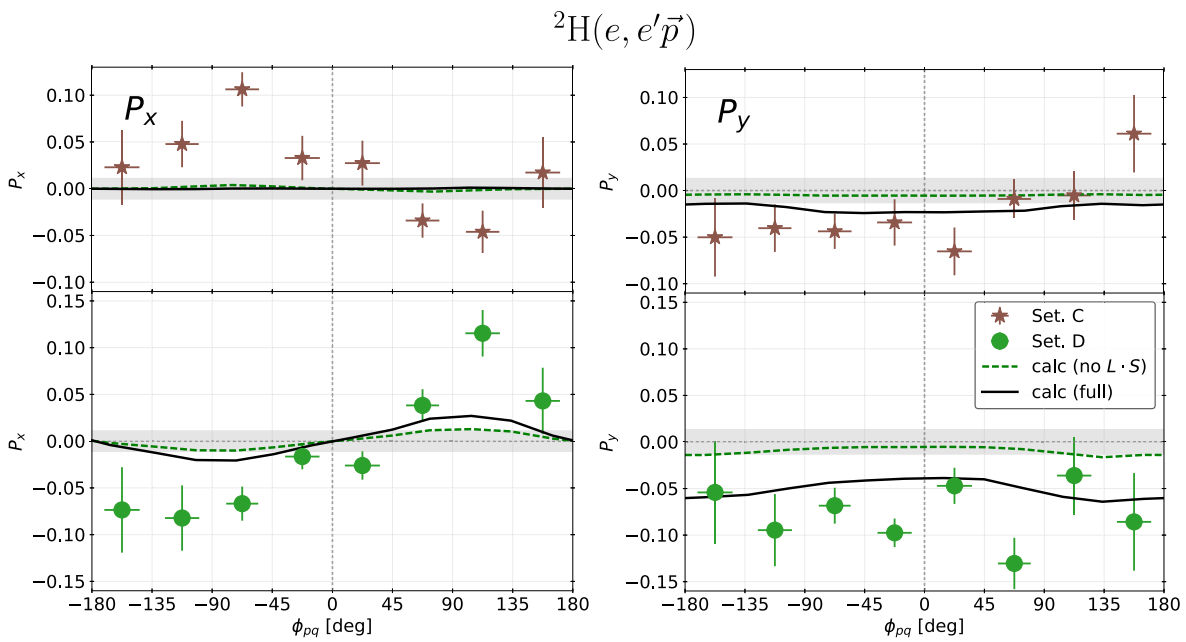

Fig. 2. Comparison of the ϕ_{pq} dependence of the measured induced polarization components P_x (left panels) and P_y (right panels) for ^{2}H to the theory for selected kinematic settings. Symbols are explained in the inset of the right bottom panel. The calculations with (without) the $L \cdot S$ potential are shown as the solid black (dashed, green online) curves. The gray band centered around y=0 represents the systematic uncertainty; see Sec. 3.3.

the size. For s-shell knockout, there is some deviation between the data and calculations, which is largest at $|\phi_{pq}|$ near 180°.

Switching off the $L \cdot S$ part of the optical potential results in much smaller or vanishing induced polarization for both components, indicating that the induced polarization originates primarily from the $L \cdot S$ part of the optical potential.

6. Missing-momentum dependence

The induced polarizations were also analyzed as functions of $p_{\rm miss}$. We note that our determination of the $p_{\rm miss}$ dependence is affected by the ϕ_{pq} dependence of the components. For P_y, the nearly flat behavior with respect to ϕ_{pq} in all regions (except for low-$p_{\rm miss}$ p-shell knockout) allows us to determine the polarization values in the $p_{\rm miss}$ bins, with little effect of the variation over ϕ_{pq}. Since P_x displays a sine-like behavior, it almost vanishes when averaged over ϕ_{pq}. Hence, one may obtain small values of P_x, even when a large-amplitude oscillation is observed. Furthermore, even a perfect sine behavior will result in a nonzero measured value when the polarization is obtained over a $p_{\rm miss}$ bin without a proper statistical weight. The values obtained for P_x for both ^{2}H and ^{12}C are shown in the supplementary material, Fig. S3. These effects are much reduced but still may exist for the P_y components.

The P_y components for ^{2}H and ^{12}C are shown in Figs. 4 and 5, respectively. For ^{2}H, the induced polarization is near zero for $p_{\rm miss} \approx 0$, where the deuteron can be considered a "weakly bound" system, and increases in magnitude with higher positive or negative $p_{\rm miss}$. Furthermore, we note this is consistent with earlier measurements of P_y from MIT [13] (open gray triangles in Fig. 4), which have near-vanishing P_y in a region near $p_{\rm miss} = 0$.

For ^{12}C we observe no significant variation of P_y over the $p_{\rm miss}$ range for s-shell protons. As observed in the ϕ_{pq}-dependence analysis, the p-shell protons show a variation with respect to $p_{\rm miss}$.

A comparison of our ^{12}C data for P_y with the earlier MIT measurements [14] is shown in Fig. S4 of the supplementary material. For this comparison, we restricted the range of ϕ_{pq} in our data sample to match that of [14] (i.e., near 180°) and compared them at the same $|p_{\rm miss}|$. The agreement between our p-shell data and those of [14] is very good, in spite of how different our kinematics are from theirs. There are some discrepancies between our data and [14] for the s-shell, particularly at small $E_{\rm miss}$ and large $|p_{\rm miss}|$. The discrepancy at large $|p_{\rm miss}|$ may be related to the fact that our high-$|p_{\rm miss}|$ setting (Setting G) has very different four-momentum transfer ($Q^2 = 0.18$ (GeV/c)^2)) from that of the MIT measurement ($Q^2 = 0.49$ (GeV/c)^2), whereas for our low $|p_{\rm miss}|$ setting (Setting A, $Q^2 = 0.40$ (GeV/c)^2), the difference in Q^2 is much smaller.

The calculations were performed as before, using the kinematics and statistics of the data in each $p_{\rm miss}$ bin. The calculations for ^{2}H show the same increasing polarization with $|p_{\rm miss}|$, and vanishing at $p_{\rm miss} = 0$ as would be expected for a "very weakly bound" proton. Overall the calculated P_y agrees well with the data except in the negative $p_{\rm miss}$ region (Settings C and D). The deviations of the calculation from the measured polarization, while small, may point to a need for a fine tuning of the NN potential. We note that there were also discrepancies between data and calculations observed in the same region of negative $p_{\rm miss}$ for the transferred polarization [18]. One may speculate that the discrepancies in the transferred and induced polarizations may be related.

For ^{12}C calculation we note the positive P_y obtained for the s-shell protons. Examining the ϕ_{pq} dependence of the calculation, we can attribute this to the fact that this event sample is dominated by events with large $|\phi_{pq}|$ (where the calculated P_y is positive). For the p shell, the agreement is good.

To describe the $p_{\rm miss}$ dependence of the P_x and P_y components for p-shell protons from ^{12}C we first obtained the ϕ_{pq} distribution for each of the $p_{\rm miss}$ bins. Then we parameterized the data assuming $P_x = a_x + b_x \sin(\phi_{pq})$ and $P_y = a_y + b_y \cos(\phi_{pq})$. The data for each bin along with the fit are shown in the supplementary materials, Figs. S5 and S6. The "amplitudes" (b_x and b_y) are shown in Fig. 6.

Both, P_x and P_y show a similar behavior of increasing amplitudes towards small $p_{\rm miss}$ (reaching values of ≈ -0.3 and ≈ 0.4 respectively), and become small at large $p_{\rm miss}$. However, the rise for b_y as $p_{\rm miss}$ approaches zero appears to be sharper than that of b_x.

We note that the amplitudes b_x and b_y are of opposite signs, negative and positive respectively, and that their magnitudes are

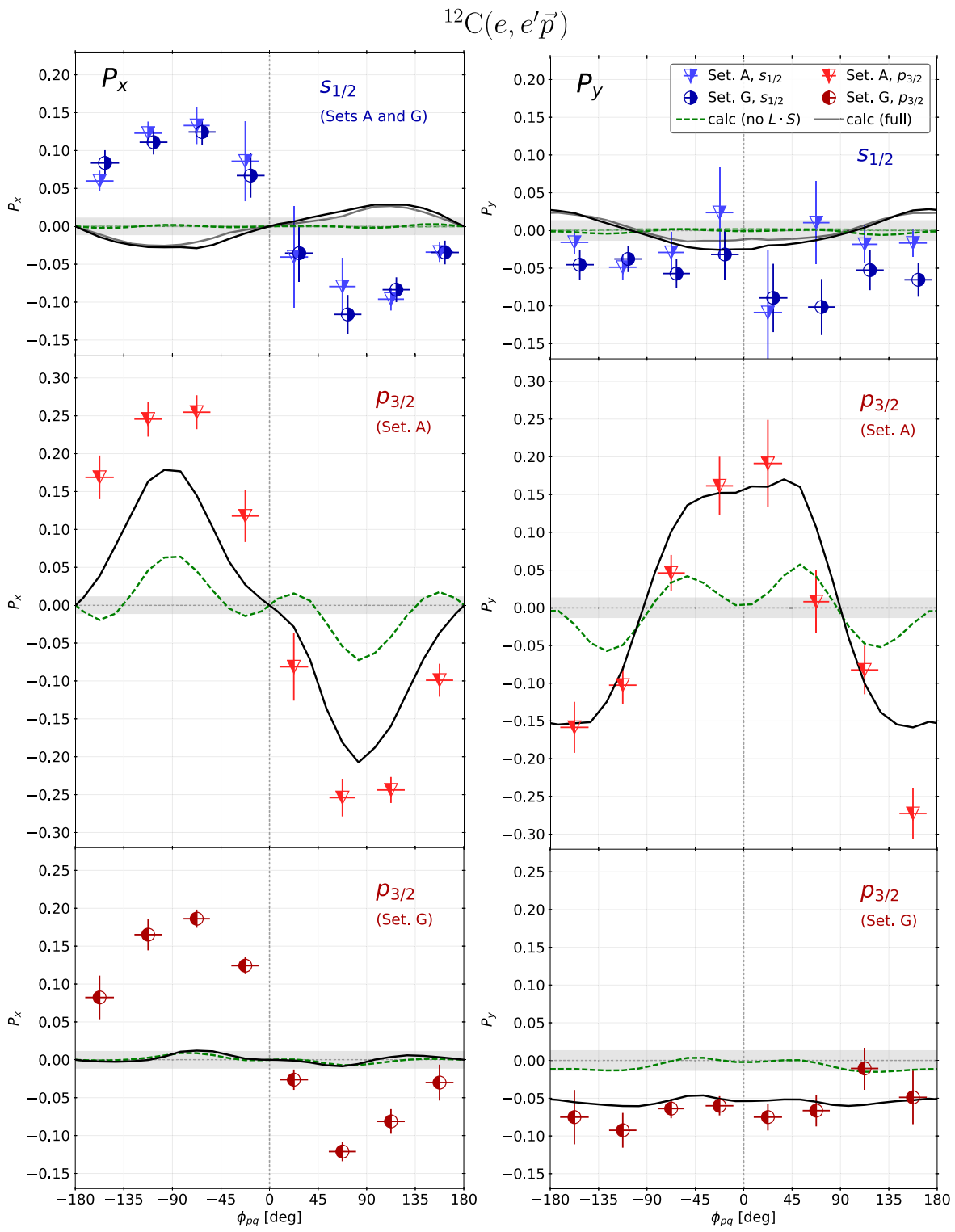

Fig. 3. For ^{12}C, the ϕ_{pq} dependence of the measured polarization components P_x (left panels) and P_y (right panels) compared to theory. These are shown for s-shell knockout for both kinematic settings (top panels), and for p-shell knockout at small p_{miss} (Setting A, middle panels) and large negative p_{miss} (Setting G, bottom panels). Calculations with (without) the $L \cdot S$ part of the optical potential are shown as solid black (dashed, green online) curves. In the top panels, the curves for Setting A are shown in gray (light green online for no-$L \cdot S$) in order to contrast with those of Setting G.

similar at low $|p_{\mathrm{miss}}|$. Our results are presented with respect to the coordinate system in the scattering plane (see Fig. 1). In the low-$|p_{\mathrm{miss}}|$ region, they seem to be consistent with projections of a vector which is normal to the *reaction* plane on the x and y axes defined in the *scattering*-plane coordinate system, which are proportional to $-\sin(\phi_{pq})$, and $\cos(\phi_{pq})$ respectively.

7. Conclusions

We have measured the induced polarization components, P_x and P_y over the full azimuthal-angle range for ^{2}H and ^{12}C. The off-coplanar measurements provide new data which show the azimuthal dependence of the induced polarization components, par-

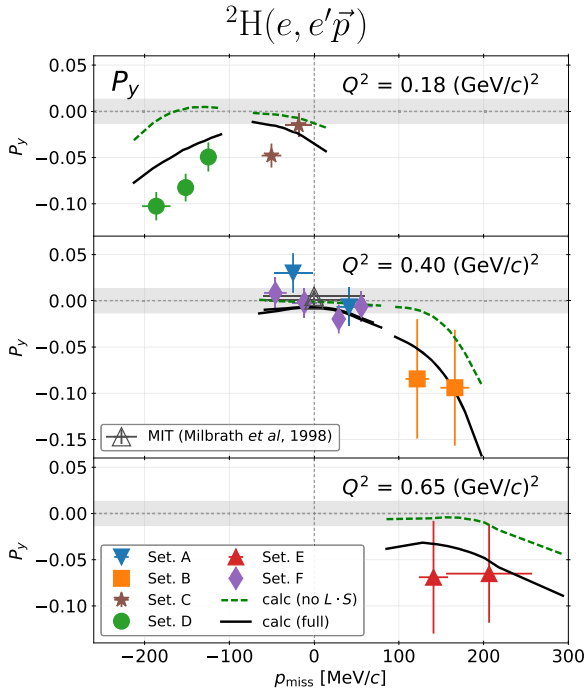

Fig. 4. The measured P_y components of the induced polarization for ^{2}H, as functions of the missing momentum. Different symbols (color online) represent different kinematic settings as shown in the inset of the lowest panel. Grey open triangles indicate the measurements from MIT-Bates [13], taken at Q^2 = 0.38 and 0.50 (GeV/c)^2, both with p_{miss} centered at zero. The uncertainties for the data points are statistical only. Theoretical results with (without) the $L\cdot S$ part of the interaction are shown as solid black (dashed, green online) curves.

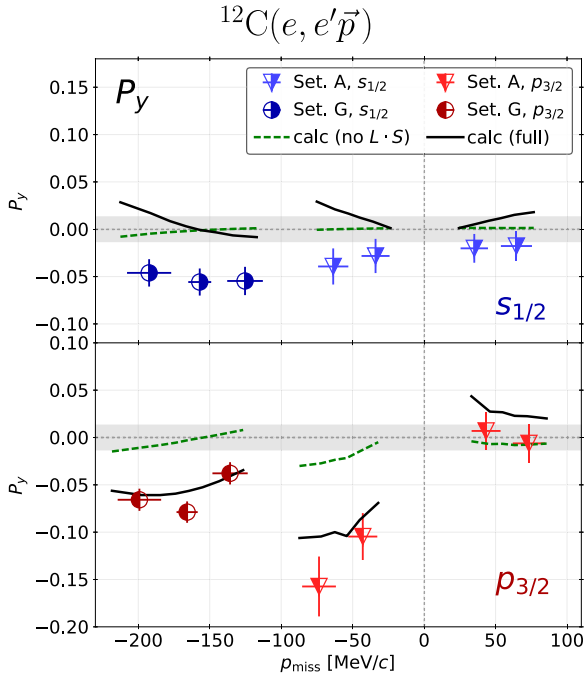

Fig. 5. The measured induced-polarization component P_y for ^{12}C as a function of the missing momentum compared to theory. Triangles (circles) refer to kinematic Setting A (G). Symbols that are open on the left (right) side refer to s-shell (p-shell) removals, and are colored blue (red) online. The calculations with (without) the $L\cdot S$ potential are shown in solid black (dashed, green online) curves.

ticular, the P_x which vanishes in coplanar kinematics. These are the first measurements of P_x, and cover a large extended kinematical range. The statistics obtained in these measurements is significantly improved over previous measurements, allowing meaningful comparison with state-of-the-art calculations. In general, the calculations are in good agreement with the measured P_y components in contrast to their predictions for P_x.

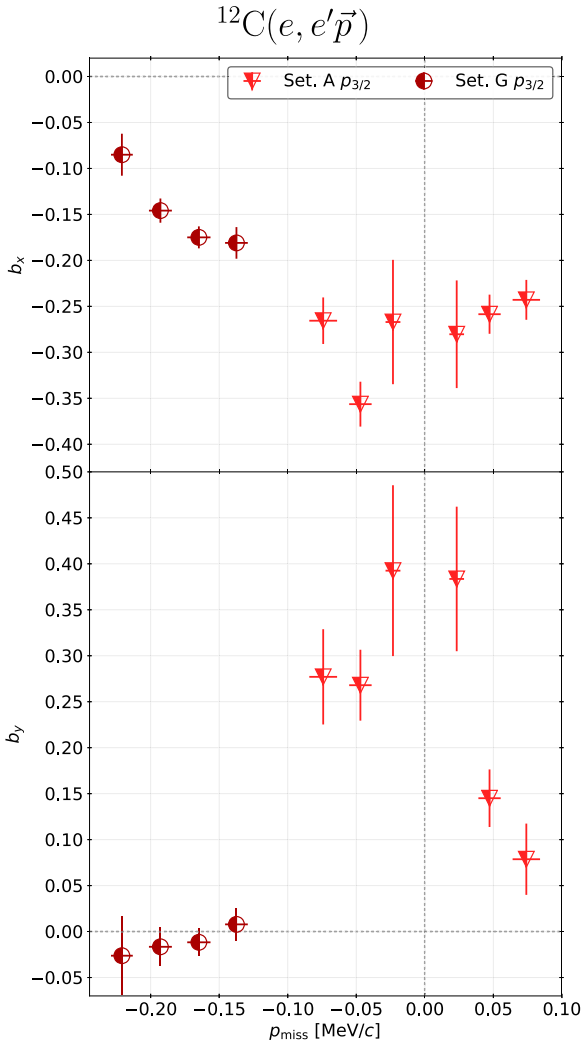

Fig. 6. The parameters b_x and b_y from the fits $P_x = a_x + b_x \sin\phi_{pq}$ and $P_y = a_y + b_y \cos\phi_{pq}$. These parameters describe the ϕ_{pq} dependence of P_x and P_y respectively.

The theoretical predictions for P_x in both nuclei are considerably smaller than the measured data and in some cases have the opposite sign. The fact that induced P_x is not well described in the calculations has probably little effect on the prediction of other measured polarization observables (which are coplanar or integrated over the azimuthal angle).

For ^{12}C, the calculations for the p-shell knockout are in better agreement with the data than those for the s shell. This may indicate that the transitions to discrete eigenstates of the residual nucleus may be better described by the theoretical calculations than the s-shell knockout with final states in the continuum. The large polarization values observed in ^{12}C near $p_{miss} = 0$ (for both, P_y and P_x oscillation amplitudes) may be attributed to the minimum in the momentum distribution of the p-shell protons. A singular steep minimum may affect polarization observables. This may be also the reason for the enhanced oscillations of P_x near $p_{miss} = 0$. The P_y component, which vanishes in PWIA, is entirely due to final-state interactions, and, as shown, stems mainly from the spin-orbit part of the optical or the nucleon-nucleon potentials, in ^{12}C and ^{2}H, respectively.

The new data presented in this work provide a new and more detailed testing ground for theoretical models of the nucleon-nucleon interaction and nuclear structure.

Declaration of competing interest

The authors declare that they have no known competing financial interests or personal relationships that could have appeared to influence the work reported in this paper.

Acknowledgements

We would like to thank the Mainz Microtron operators and technical crew for the excellent operation of the accelerator. This work is supported by the Israel Science Foundation (Grants 390/15, 951/19) of the Israel Academy of Arts and Sciences, by the Israel Ministry of Science, Technology and Spaces, by the PAZY Foundation (Grant 294/18), by the Deutsche Forschungsgemeinschaft (Collaborative Research Center 1044), by the U.S. National Science Foundation (PHY-1205782, PHY-1505615), by the United States-Israeli Binational Science Foundation (BSF) as part of the joint program with the NSF (Grant 2017630), and by the Croatian Science Foundation Project No. 8570. We acknowledge the financial support from the Slovenian Research Agency (research core funding No. P1–0102).

Appendix A. Supplementary material

Supplementary material related to this article can be found online at https://doi.org/10.1016/j.physletb.2020.135984.

References

[1] M.G. Mayer, Nuclear configurations in the spin-orbit coupling model. I. Empirical evidence, Phys. Rev. 78 (1950) 16–21, https://doi.org/10.1103/PhysRev.78.16.
[2] O. Sorlin, M.-G. Porquet, Nuclear magic numbers: new features far from stability, Prog. Part. Nucl. Phys. 61 (2) (2008) 602–673, https://doi.org/10.1016/j.ppnp.2008.05.001.
[3] O. Haxel, J.H.D. Jensen, H.E. Suess, On the "magic numbers" in nuclear structure, Phys. Rev. 75 (1949) 1766, https://doi.org/10.1103/PhysRev.75.1766.2.
[4] S. Boffi, C. Giusti, F. Pacati, Spin-orbit distortion of the emerging nucleon in quasi-free electron scattering, Nucl. Phys. A 336 (3) (1980) 437–445, https://doi.org/10.1016/0375-9474(80)90220-1.
[5] C. Giusti, F.D. Pacati, Complete determination of scattering amplitudes and nucleon polarization in electromagnetic knockout reactions, Nucl. Phys. A 504 (1989) 685–711, https://doi.org/10.1016/0375-9474(89)90003-1.
[6] S. Boffi, C. Giusti, F.d. Pacati, M. Radici, Electromagnetic Response of Atomic Nuclei, Oxford Studies in Nuclear Physics, vol. 20, Clarendon Press, Oxford UK, 1996.
[7] A. Meucci, C. Giusti, F.D. Pacati, Relativistic corrections in (e, e-prime p) knockout reactions, Phys. Rev. C 64 (2001) 014604, https://doi.org/10.1103/PhysRevC.64.014604, arXiv:nucl-th/0101034.
[8] J.R. Vignote, M.C. Martínez, J.A. Caballero, E. Moya de Guerra, J.M. Udias, $a(\vec{e}, e'\vec{p})b$ responses: from bare nucleons to complex nuclei, Phys. Rev. C 70 (2004) 044608, https://doi.org/10.1103/PhysRevC.70.044608.
[9] L.L. Lee, J.P. Schiffer, Experimental evidence for j dependence of the angular distribution from (d, p) reactions, Phys. Rev. Lett. 12 (1964) 108–110, https://doi.org/10.1103/PhysRevLett.12.108.
[10] J.P. Schiffer, L.L. Lee, A. Marinov, C. Mayer-Böricke, Dependence of the angular distribution of the (d, p) reaction on the total angular-momentum transfer. II, Phys. Rev. 147 (1966) 829–835, https://doi.org/10.1103/PhysRev.147.829.
[11] Y. Horikawa, M. Thies, F. Lenz, The δ-nucleus spin-orbit interaction in π-nucleus scattering, Nucl. Phys. A 345 (2) (1980) 386–408, https://doi.org/10.1016/0375-9474(80)90346-2.
[12] S. Watanabe, High energy scattering of deuterons by complex nuclei, Nucl. Phys. 8 (1958) 484–492, https://doi.org/10.1016/0029-5582(58)90180-9.
[13] B.D. Milbrath, J.I. McIntyre, C.S. Armstrong, D.H. Barkhuff, W. Bertozzi, J. Chen, others Bates FPP Collaboration, A comparison of polarization observables in electron scattering from the proton and deuteron, Phys. Rev. Lett. 80 (1998) 452–455, https://doi.org/10.1103/PhysRevLett.80.452, Erratum: Phys. Rev. Lett. 82 (1999) 2221, https://doi.org/10.1103/PhysRevLett.82.2221, arXiv:nucl-ex/9712006.
[14] R. Woo, et al., Measurement of the induced proton polarization P_n in the $^{12}C(e, e'\vec{p})$ reaction, Phys. Rev. Lett. 80 (1998) 456, https://doi.org/10.1103/PhysRevLett.80.456.
[15] S. Strauch, S. Dieterich, et al., Polarization transfer in the $^4He(\vec{e}, e'\vec{p})^3H$ reaction up to $Q^2 = 2.6$ (GeV/c)^2, Phys. Rev. Lett. 91 (2003) 052301, https://doi.org/10.1103/PhysRevLett.91.052301.
[16] S.P. Malace, M. Paolone, S. Strauch, I. Albayrak, J. Arrington, B.L. Berman, E.J. Brash, B. Briscoe, A. Camsonne, J.-P. Chen, et al., Precise extraction of the induced polarization in the $^4He(e, e'\vec{p})^3H$ reaction, Phys. Rev. Lett. 106 (5) (2011), https://doi.org/10.1103/physrevlett.106.052501.
[17] I. Yaron, D. Izraeli, et al., Polarization-transfer measurement to a large-virtuality bound proton in the deuteron, Phys. Lett. B 769 (2017) 21–24, https://doi.org/10.1016/j.physletb.2017.01.034.
[18] D. Izraeli, I. Yaron, et al., Components of polarization-transfer to a bound proton in a deuteron measured by quasi-elastic electron scattering, Phys. Lett. B 781 (2018) 107–111, https://doi.org/10.1016/j.physletb.2018.03.063, arXiv:1801.01306.
[19] S. Paul, D. Izraeli, T. Brecelj, I. Yaron, et al., Polarization-transfer measurements in deuteron quasi-elastic anti-parallel kinematics, Phys. Lett. B 795C (2019) 599–605, https://doi.org/10.1016/j.physletb.2019.07.002, arXiv:1905.05594.
[20] D. Izraeli, T. Brecelj, et al., Measurement of polarization-transfer to bound protons in carbon and its virtuality dependence, Phys. Lett. B 781 (2018) 95–98, https://doi.org/10.1016/j.physletb.2018.03.027, arXiv:1711.09680.
[21] T. Brecelj, S.J. Paul, T. Kolar, et al., Polarization transfer to bound protons measured by quasielastic electron scattering on ^{12}C, Phys. Rev. C 101 (2020) 064615, https://doi.org/10.1103/PhysRevC.101.064615.
[22] T. Kolar, S. Paul, T. Brecelj, et al., Comparison of recoil polarization in the $^{12}C(\vec{e}, e'\vec{p})$ process for protons extracted from s and p shell, Phys. Lett. B (2020) 135903, arXiv:2007.14985, https://doi.org/10.1016/j.physletb.2020.135903.
[23] K. Blomqvist, et al., The three-spectrometer facility at MAMI, Nucl. Instrum. Methods A 403 (2–3) (1998) 263–301, https://doi.org/10.1016/S0168-9002(97)01133-9.
[24] T. Pospischil, et al., The focal plane proton-polarimeter for the 3-spectrometer setup at MAMI, Nucl. Instrum. Methods Phys. Res., Sect. A 483 (3) (2002) 713–725, https://doi.org/10.1016/S0168-9002(01)01955-6.
[25] D. Dutta, et al., Quasielastic $(e, e'p)$ reaction on ^{12}C, ^{56}Fe, and ^{197}Au, Phys. Rev. C 68 (2003) 064603, https://doi.org/10.1103/PhysRevC.68.064603.
[26] E. Aprile-Giboni, R. Hausammann, E. Heer, R. Hess, C. Lechanoine-Leluc, W. Leo, S. Morenzoni, Y. Onel, D. Rapin, Proton-carbon effective analyzing power between 95 and 570 MeV, Nucl. Instrum. Methods 215 (1983) 147–157, https://doi.org/10.1016/0167-5087(83)91302-9.
[27] M.W. McNaughton, et al., The p-C analyzing power between 100 and 750 MeV, Nucl. Instrum. Methods A 241 (1985) 435–440, https://doi.org/10.1016/0168-9002(85)90595-9.
[28] H. Arenhövel, W. Leidemann, E.L. Tomusiak, General survey of polarization observables in deuteron electrodisintegration, Eur. Phys. J. A 23 (2005) 147–190, https://doi.org/10.1140/epja/i2004-10061-5.
[29] R.B. Wiringa, V.G.J. Stoks, R. Schiavilla, Accurate nucleon-nucleon potential with charge-independence breaking, Phys. Rev. C 51 (1995) 38–51, https://doi.org/10.1103/PhysRevC.51.38.
[30] J.C. Bernauer, M.O. Distler, J. Friedrich, T. Walcher, P. Achenbach, C. Ayerbe-Gayoso, et al., Electric and magnetic form factors of the proton, Phys. Rev. C 90 (1) (2014) 015206, https://doi.org/10.1103/PhysRevC.90.015206.
[31] T. De Forest, Off-shell electron-nucleon cross sections: the impulse approximation, Nucl. Phys. A 392 (2) (1983) 232–248, https://doi.org/10.1016/0375-9474(83)90124-0.
[32] M. Sharma, M. Nagarajan, P. Ring, Rho meson coupling in the relativistic mean field theory and description of exotic nuclei, Phys. Lett. B 312 (4) (1993) 377–381, https://doi.org/10.1016/0370-2693(93)90970-S.
[33] E.D. Cooper, S. Hama, B.C. Clark, Global Dirac optical potential from helium to lead, Phys. Rev. C 80 (2009) 034605, https://doi.org/10.1103/PhysRevC.80.034605.